



UNIVERSITY OF LEEDS

This is a repository copy of *Pyrolysis-catalysis of different waste plastics over Fe/Al₂O₃ catalyst: High-value hydrogen, liquid fuels, carbon nanotubes and possible reaction mechanisms*.

White Rose Research Online URL for this paper:
<https://eprints.whiterose.ac.uk/170442/>

Version: Accepted Version

Article:

Cai, N, Li, X, Xia, S et al. (7 more authors) (2021) Pyrolysis-catalysis of different waste plastics over Fe/Al₂O₃ catalyst: High-value hydrogen, liquid fuels, carbon nanotubes and possible reaction mechanisms. *Energy Conversion and Management*, 229. 113794. ISSN 0196-8904

<https://doi.org/10.1016/j.enconman.2020.113794>

© 2020, Elsevier. This manuscript version is made available under the CC-BY-NC-ND 4.0 license <http://creativecommons.org/licenses/by-nc-nd/4.0/>.

Reuse

This article is distributed under the terms of the Creative Commons Attribution-NonCommercial-NoDerivs (CC BY-NC-ND) licence. This licence only allows you to download this work and share it with others as long as you credit the authors, but you can't change the article in any way or use it commercially. More information and the full terms of the licence here: <https://creativecommons.org/licenses/>

Takedown

If you consider content in White Rose Research Online to be in breach of UK law, please notify us by emailing eprints@whiterose.ac.uk including the URL of the record and the reason for the withdrawal request.



eprints@whiterose.ac.uk
<https://eprints.whiterose.ac.uk/>

**High-value hydrogen, liquid fuels and carbon nanotubes from the
pyrolysis-catalysis of different types of waste plastics over Fe/Al₂O₃ catalyst**

Ning Cai¹, Xiaoqiang Li¹, Sunwen Xia¹, Lin Sun¹, Xiong Zhang¹, Pietro Bartocci², Hanping Chen¹,

Paul T. Williams³, Haiping Yang^{1*}

¹*State Key Laboratory of Coal Combustion, School of Energy and Power Engineering, Huazhong University of Science and Technology, Wuhan, 430074, PR China*

²*Department of Engineering, University of Perugia, via G. Duranti 67, 06125, Perugia, Italy*

³*School of Chemical and Process Engineering, University of Leeds, Leeds, LS2 9JT UK*

Abstract: The Pyrolysis-catalysis of different types of waste plastics was investigated in the presence of Fe/Al₂O₃ catalyst with the aim of producing high value hydrogen, aromatic chemicals and carbon nanotubes. Polypropylene (PP), high density polyethylene (HDPE), low density polyethylene (LDPE), high impact polystyrene (HIPS) and general-purpose polystyrene (GPPS) were used as the feedstock. The results showed that HIPS waste plastic led to a higher solids deposition yield of 49.4 wt.%, followed by GPPS (48.7 wt.%), HDPE (36.9 wt.%), LDPE (35.9 wt.%) and PP (30.2 wt.%). Physical and chemical analysis of the solid deposits revealed that all specimens contained carbon nanotubes (CNTs). HIPS and GPPS exhibited relatively lower gaseous product yield, however, the polyolefin plastics produced more gaseous products, with the gaseous yield from PP, HDPE and LDPE being more than 40 wt.%. The gaseous products contained high levels of H₂, especially for PS (~74.1 vol.%). For, liquid oil, product the yield for all samples was ~20% and were composed of aromatic hydrocarbons with a carbon number range mainly between 8 and 16.

Keywords: Waste plastics; Fe based catalysts; Hydrogen; Aromatic hydrocarbons; Carbon nanotubes

1 Introduction

It has been reported that about 335 million tonnes plastics products were produced worldwide in 2016 [1], while over 20 wt.% (77 million tonnes) was manufactured in China in the same year [2]. Plastics are used in a wide variety of applications including packaging, household, leisure and sports equipment and in various industrial sectors such as industry, building and construction, electrical and electronics, automobile and automotive [1].

Many plastics have a short life and generally end up as part of the municipal solid waste (MSW) stream, which may be incinerated or disposed to landfills [3] with only 9 % being recycled [4]. The low level of plastics recycling results in a huge waste of resources. There are many types of waste plastics found in MSW, among which polyolefin plastics accounts for the highest fraction, consisting of 20 wt.% polypropylene (PP), 17.4 wt.% high density polyethylene (HDPE) and 20.6 wt.% low density polyethylene (LDPE). Other commonly found plastics in MSW include high impact polystyrene (HIPS), general purpose polystyrene (GPPS) polyethylene terephthalate and polyvinyl chloride [5,6].

There has been recent interest in the conversion of waste plastics into high value products using the thermochemical process of pyrolysis-catalysis as a promising technology for utilization of wastes plastic [7]. Different kinds of plastics have been investigated to produce various high-value products like synthesis gas [8-10], liquid chemicals [11-13] or carbon nano-materials [14-16]. Wu et al. [17] produced more

syngas with a high volume fraction of hydrogen (over 60 vol.%) from PP plastics using pyrolysis-catalysis with steam reforming at a catalyst temperature of ~800 °C. Alternatively, using a ZSM-5 catalyst at lower temperature (~500 °C) a product oil may be produced producing for example, light olefins from HDPE or aromatic hydrocarbon from PS. For example, Park et al. [18] produced a liquid oil from the pyrolysis-catalysis of PS that contained 26.3 wt.% monocyclic aromatic hydrocarbons: benzene, toluene, ethylbenzene and xylenes (BTEX). More recently, some research has focused on liquid chemicals for jet fuel obtained from activated carbon [12] or activated carbon and MgO [19]. In addition, Fe/carbon nanotube nano-composites with high value were also produced from waste plastics by Zhang et al. [20]. Furthermore, co-production of H₂ and CNTs, was carried out by Nahil et al. [14] and Yao et al. [21].

Notably, pyrolysis-catalysis products of the waste plastics depend on the intrinsic structure of the plastic to a great extent and work has been carried out for the comparison of different products from different types of plastics. For example, Saad et al. [22] studied the pyrolysis-catalytic reforming of various types of waste plastics and found that the order was LDPE < HDPE < PP < PS in terms of syngas yield. Miandad et al. [23] reported that liquid from the pyrolysis-catalysis of several types of plastic waste consisted of mainly aromatic hydrocarbons such as benzene, toluene, ethylbenzene, styrene and naphthalene. In relation to carbon nanotubes (CNTs) production from different plastics, Aboul-Enein et al. found that CNTs with higher purity and quality could be produced from LDPE or PP waste using a commercial catalyst [24]. To further the pyrolysis-catalysis process for the production of high value products, it is of

interest to explore the catalytic thermal conversion process of different types of waste plastics is, especially the cooperative and competitive mechanism between product formation.

Therefore, the aim of the current work is to identify the thermal conversion process and possible reaction mechanism of different types of waste plastics (PP, LDPE, HDPE, HIPS and GPPS) in the presence of a catalyst. The yield and composition of the gaseous and liquid products, the morphological structure and quality of the obtained carbon nanomaterials were investigated.

2 Materials and methods

2.1 Materials

The plastics samples used were polypropylene (PP), high density polyethylene (HDPE), low density polyethylene (LDPE), high impact polystyrene (HIPS) and general purpose polystyrene (GPPS). The corresponding proximate and ultimate analysis of the plastics are presented in **Table 1**. and show that, PP, HDPE and LDPE contain ~ 85 wt.% C and ~ 14 wt.% H. Whereas, HIPS and GPPS contain over 91 wt.% C, but less H (~ 7wt.%). For all samples, the volatile matter content exceeded 99.5 wt.% and less than 0.1 wt.% ash was detected.

The catalyst preparation used iron nitrate nonahydrate ($\text{FeNO}_3 \cdot 9\text{H}_2\text{O}$) and nano-aluminium oxide (Al_2O_3) with particle size of 10nm purchased from Sigma Aldrich (China). Absolute ethyl alcohol was purchased from Sinopharm Chemical Reagent Co. Ltd. (China). All chemicals were of analytical grade and used without any

further purification. The Fe-based catalyst used for the pyrolysis-catalysis experiments was prepared using an impregnation method according to our previous work [25]. Briefly, 0.72 g $\text{FeNO}_3 \cdot 9\text{H}_2\text{O}$ was dissolved in 30 mL absolute ethyl alcohol with continuous stirring until completely dissolved, then 0.9 g nano- Al_2O_3 was introduced into the iron salt solution to ensure an Fe loading content of 10 wt.% was achieved. The solution mixture was stirred with a magnetic stirrer at a temperature of 50 °C until the solution becoming a slurry. The slurry was then oven drying for 12 h at 105 °C to remove the absolute ethyl alcohol. The obtained dry solid was ground into small particles of size between 0.08 and 0.16 mm, followed by calcination at a final temperature of 800 °C for 2 h with a heating rate of 20 °Cmin⁻¹ in an air atmosphere in a muffle furnace. After natural cooling to room temperature (~25 °C), the produced Fe/ Al_2O_3 catalyst was stored until use.

2.2 Pyrolysis-catalysis experimental system

The pyrolysis-catalysis of the different waste plastics using the Fe/ Al_2O_3 catalyst was carried out in a two-stage vertical fixed bed quartz reactor. A schematic diagram of the reactor system is shown in **Fig. 1**. The quartz reactor was heated by two separate electrical furnaces, each separately monitored and controlled to provide a heated pyrolysis zone and a separate heated catalysis zone. The pyrolysis of the plastics involved heating the sample from ambient temperature to a final pyrolysis temperature of 500 °C, whereas the catalyst temperature was maintained at 800 °C. Nitrogen was used as the purge gas with a gas flow velocity of 100 mL min⁻¹. For

each experiment 1.0 g of the plastic sample was placed in a crucible in the first stage pyrolysis reactor and 0.5 g of Fe/Al₂O₃ catalyst was placed into a quartz crucible in the catalyst stage and preheated to 800 °C. Once the target temperature of the catalytic stage was reached, the pyrolytic stage was heated to 500 °C with a heating rate of 10°C min⁻¹ and kept isothermal for 10 min. In order to collect liquid oil products and gaseous products effectively, they were collected separately from repeated experiments. For the effective accurate collection of gases an ice water condensing system was used followed by gas collection in a gas sample bag. For the effective and accurate collection of liquid products, the condensation system consisted of a liquid nitrogen trap. The solid deposited carbonaceous material deposited in the catalytic reactor crucible holding the catalyst was collected for later analysis. The carbon deposition yield was determined from the the weight difference of the quartz crucible holding the catalyst before and after reaction. The liquid product yield was computed from the difference of initial and final weight of the condensate bottle in liquid nitrogen condenser. For gaseous yield, the yield was obtained from gas density and gas volume fraction after accounting for the nitrogen purge gas. Each sample was tested at least three times to ensure the accuracy of the experiment, and final results were taken from the average data of three sets with an error less than 5%.

2.3 Characterization of catalyst and pyrolysis-catalysis products.

The fresh prepared Fe/Al₂O₃ catalyst, was characterised in relation to its physical and chemical properties using several techniques. Scanning electron microscopy (SEM) was used to observe the surface morphology of the Fe/Al₂O₃ catalyst using a Gemini Sigma 300 (Carl Zeiss AG corporation, Germany), and the test voltage was set as 2.00 kV. X-ray diffraction (XRD) (Philips X'Pert PRO, Japan) was used to determine the crystalline structure and active metal catalyst particle size. Scanning range and scanning speed were 10–80° and 7° min⁻¹, respectively. A nitrogen adsorption measurement system (Quantachrome IQ, China) was used to explore the physical structure at 77 K involving the Brunauer Emmett Teller (BET) theory, including specific surface areas, total pore volumes, and pore size distribution.

Gas chromatography (GC) (Panna A91, China) was used to determine the gaseous products with two different modules, thermal conductivity detector (TCD) and flame ionization detector (FID). They were equipped to separate and analyze as many species as possible in the gaseous products. After accounting for nitrogen, the relative volume of the gaseous compounds yield was calculated. The Eq. (1) was used to calculate the gaseous products low heating value (LHV):

$$\text{LHV}(\text{MJ}/\text{Nm}^3) = 0.126 \times \text{CO} + 0.108 \times H_2 + 0.358 \times CH_4 + 0.665 \times C_nH_m \quad (1)$$

Gas chromatography-mass spectroscopy (GC/MS, HP7890 series GC with a HP5975MS detector) was used to identify the components in the liquid product with a HP-5MD capillary column. And the organic components were further determined by

mass spectral libraries (NIST14.L).

For the characterisation of the carbon deposits on the catalyst after pyrolysis-catalysis of the waste plastics, Transmission electron microscopy (TEM) and high resolution TEM (HR-TEM) were used to observe and visualize the surface morphology and size of the carbon nanomaterial deposits with a field-emission transmission electron microscope (Tecnai G2 F20 S-TWIN) at an accelerating voltage of 200 kV. The used catalyst containing the carbon deposits was analysed using temperature programmed oxidation (TPO). Thermogravimetric analysis (TGA) of the catalyst was carried out on a Diamond TG/DTA to determine the oxidation profile of the deposited carbons in relation to TGA temperature. The crystal structure of the carbon deposits was also determined by XRD and size of the carbon deposits and iron particles (D_C and D_{Fe}) was calculated by Scherrer equation (Eq. (2)), based on the (002) and (110) peak, respectively. The interlayer spacing (d_{002}) of the carbon deposits was calculated from Bragg's equation (Eq. (3)). Furthermore, the graphitization degree parameter (g^d) and the number of carbon layers (N) were evaluated by the interlayer spacing. In addition, the degree of graphitization of the carbon deposits was also examined by Raman spectrometry with Raman spectra from 800 cm^{-1} to 3200 cm^{-1} on a LabRAM HR 800 Evolution Raman instrument with an excitation wavelength of 532 nm.

$$D = k\lambda/\beta\cos\theta \quad (2)$$

$$d_{002} = n\lambda/2\sin\theta \quad (3)$$

3 Results and discussion.

3.1 Fresh catalysts

The fresh Fe/Al₂O₃ catalyst, was characterised in relation to its surface area and porosity. The adsorption/desorption curve, physical structure parameters and pore size distribution of the Fe/Al₂O₃ catalyst are presented in **Fig. 2(a)** and **2(b)**. As shown in **Fig. 2(a)**, the Fe/Al₂O₃ catalyst exhibited a blend of type II and IV isotherms, which suggest the widespread presence of mesoporous and macroporous. Adsorbing capacity increased rapidly at high relative pressure regions was related to macroporous material [26]. Furthermore, typical H3 hysteresis loops were observed at relative pressure in the range 0.7–0.9. H3 hysteresis loops are often seen in mesoporous materials, and this is the characteristic of slit shaped pores formed by the accumulation of flake particles [27]. The pore size distribution shown in **Fig. 2(b)** also revealed the existence of a large number of mesoporous and all the pore diameters were larger than 7 nm. In addition, specific surface areas, total pore volumes and average diameter of the catalyst metal particles were also obtained from nitrogen adsorption/desorption test and they were 96.78 m² g⁻¹, 0.62 cm³g⁻¹ and 25.78 nm, respectively.

The morphology of the fresh catalyst was analyzed by SEM, shown in **Fig. 2(c)**. The size of the iron catalyst prepared by the impregnation method could reach hundreds of nanometers. It appeared that the catalyst was made up of many small particles in a loose structure, which could be the source of the porous inner structure. The small particles might be attributed to the nano-aluminium oxide support. This kind of

structure with small particles was reported to be beneficial for active metal diffusion inside of the catalyst, which favours the promotion of catalyst activity [28].

The fresh catalyst was further analysed by XRD, as showed in **Fig. 2(d)**. The peak at 2θ , 32.8° corresponding to the (4 2 0) plane, confirmed the presence of Fe_2O_3 (Reference code: 00-016-0653). The other several peaks at 2θ , 31.2° , 36.5° , 44.7° , 47.1° , 60.0° and 67.3° were related to the aluminium oxide support. In addition, the average crystallite size of Fe_2O_3 was 26.24 nm, calculated from the peak at around 2θ , 32.8° according to the Scherrer-equation. This indicates good dispersion of the active Fe species prepared by impregnation.

3.2 Influence of wastes plastics type on product yield and composition

3.2.1 Yield of pyrolysis-catalysis products

The pyrolysis-catalysis of the different types of waste plastic was undertaken using the two-stage fixed bed quartz reactor. The product yield in relation to polypropylene (PP), high density polyethylene (HDPE), low density polyethylene (LDPE), high impact polystyrene (HIPS) and general-purpose polystyrene (GPPS) are shown in **Fig. 3**.. It can be seen that the distribution of products from the pyrolysis-catalysis of the different plastics varied with the type of plastic used as feedstock. PP produced a lower yield of catalyst carbon deposits (~ 30.2 wt.%) but relatively higher yield of gaseous product (~ 41.7 wt.%). Compared with PP, the carbon deposits from the PE structured plastics increased by about 20%, reaching 36.9 wt.% and 35.9 wt.% for HDPE and LDPE, respectively. Hernadi et al. found that propylene was not as reactive as ethylene during

a catalytic process for the production of carbon nanotubes [29]. It was suggested that plastic polymers decompose through random scission at high temperature, the ethylene from PE degradation was more actively involved in the catalytic coke deposition than propylene produced from PP, leading to the increase of solid carbon. **Fig. 3** shows that for HIPS and GPPS, the amount of deposited carbon was about 50 wt.%, which was over 10 wt.% more than that from pyrolysis-catalysis of the polyolefin plastics. This was related to the difference in the molecular structure of the different plastics, since there is an abundance of benzene rings on the main polymer structure of HIPS and GPPS, which are the basic unit structure of carbon. When HIPS and GPPS were heated to the decomposition temperature, the large polymer molecules break up into small aromatic molecules such as styrene and styrene oligomers. In the presence of catalysts, the ethenyl in styrene is removed resulting in benzene rings available for the direct formation of aromatic hydrocarbons [30] and carbon. Simultaneously, C-C and C-H bonds in ethenyl were further broken. On the catalyst, the carbon atoms are dissolved and recombined by melting iron, forming graphitic carbon. The remaining hydrogen atoms combine to form low molecular weight gases. Compared with micromolecule alkane and olefin, the heavier aromatic hydrocarbon compounds play an important role in the carbon generation process [31]. Furthermore, due to the higher transformation of carbon into a solid carbon, the yield of gaseous products from PS was much lower than that from PP and PE. Similar results were reported by other researchers indicating that a higher gaseous yield was attributed to the thermal degradation of polyolefin such as PE [32]. In addition, a higher yield of liquid oil was obtained from GPPS (26.1 wt.%),

producing over 5 wt.% more than that from HIPS. The difference of liquid yield from GPPS compared with HIPS could be ascribed to the absence of polybutadiene in GPPS that led to an increase of polycyclic aromatic hydrocarbons during pyrolysis-catalysis.

3.2.2 Composition of gaseous products

Fig. 4. shows the volume fractions of the gaseous components for pyrolysis-catalysis of different types waste plastics. Significant differences could be observed in the relative proportions of the gaseous products in relation to the plastics used. As can be seen from **Fig. 4**, the gaseous product from the pyrolysis-catalysis of PP mainly contained H₂, CH₄, CO and C₂H₄, and the corresponding content was 58.7, 32.4, 4.2 and 3.7 vol.%, respectively. In addition, a small amount of C₂H₆ and other gases (e.g. C₃H₆) were detected. Pyrolysis-catalysis of HDPE and LDPE produced less hydrogen and more hydrocarbons. However, HIPS and GPPS, produced a product gas with significantly higher hydrogen content compared to the other plastics, for example, the highest volume percent of hydrogen was obtained with HIPS at 74.1 vol.%. This is consistent with the product yield results for HIPS (and also GPPS) shown in **Fig. 3** where more carbon was deposited on the catalyst, and the hydrogen atoms were released in the form of hydrogen gas. Accordingly, the more light hydrogen gas that was produced also led to the reduction in the total mass fraction of the gaseous product. The high abundance of hydrogen makes it possible for further high-value applications after purification or refinement. For example, high purity hydrogen has an important application potential for use in fuel cells [33] or aviation fuel. The low heating values

(LHV) of the gaseous products were calculated. The LHV of the gases from PP and PE were over 20 MJm^{-3} , which suggests the gas could be used as industrial fuel gas directly to fuel the process [34]. In addition, although the LHV of the gases from HIPS and GPPS was lower ($\sim 15 \text{ MJm}^{-3}$), it could also be used as fuel gas.

3.2.3 Composition of the liquid products

The composition of the liquid product analysed by GC/MS from the pyrolysis-catalysis of the different plastics are presented in **Fig. 5**. The liquid product components were grouped according to carbon number, and the percentage and corresponding compound are also shown in **Fig. 5**. The carbon number distribution of the liquid products varied from 6 to 22. In particular for PP and PE, the components in the liquid product of carbon number less than 9 could hardly be detected. While for components with a carbon number larger than 9, different polyaromatic hydrocarbons were obtained. For example, the the liquid oil from PP, produced a significantly higher proportion of naphthalene (C10) at 27.2%, followed by pyrene (C16) at 15.7%, anthracene (C14) at 15.3% and biphenyl (C12) at 12.7%. The content of the other components were all less than 10%. The liquid produced from PE produced even higher yield of naphthalene ($\sim 30\%$) and pyrene ($\sim 18\%$). The liquid oil from pyrolysis-catalysis of HDPE and LDPE showed similar composition and content, which could be related to their similar molecular structure. As shown in **Fig. 5**, it seems that the liquid product generated from PS contained more types of compounds in the C6 - C8 range compared with liquid products derived from PP or PE. A reaction

mechanism may be suggested. The thermal degradation of PP and PE promotes the cracking and random scission of the polymer chain which leads to the formation of a large number of micromolecule hydrocarbon species, such as alkenes or alkanes. In the presence of the Fe/Al₂O₃ catalyst, further cracking and deposition of the micromolecule hydrocarbon species occurs. Catalytic reforming reactions of the micromolecule hydrocarbons occurs, leading to the production of larger molecules. However, in the case of PS-type plastics (HIPS and GPPS) due to the high stability of benzene and its derivatives produced from the thermal degradation of PS, limited further cracking occurs that produces lighter hydrocarbons for the further catalytic deposition process [18]. Only the branches in the aromatic hydrocarbons are removed, which could be further degraded into C and H atoms in the presence of the Fe/Al₂O₃ catalyst. The C and H atoms acting as precursors for carbon deposition and hydrogen formation. The remaining aromatic hydrocarbons such as benzene may oligomerize to form polycyclic aromatics hydrocarbons. In addition, the widespread formation of aromatic hydrocarbons are also an important source of carbon deposition [35].

The constituents in the product liquid oil obtained from the pyrolysis-catalysis of the different plastics in the range C8 to C16 were grouped together, and the results for each plastic are shown inset into **Fig. 5**. The C8 - C16 carbon number range was chosen as this is the range for jet fuel, and thereby gives an indication of the potential of the liquid product as a fuel, particularly aviation jet fuel [12]. As can be seen from **Fig.5**, the C8- C16 constituents accounted for over 80% in the liquid products

from PP and PE, which was about 20% higher than that of HIPS and GPPS. The composition of the product oils suggest that they could be used as additives for aviation jet fuel or with further chemical refinement, could be used as jet fuel directly.

3.2.4 Analysis of the reacted catalysts

Fig. 6 shows the TEM images of the carbon catalyst coke deposits on the used catalysts from the pyrolysis-catalysis of the different waste plastics. The images confirmed that the solid carbon deposits on the surface of the used catalyst contained carbon nanotubes (CNTs). The outer diameter of the produced CNTs ranged from a few nanometers to tens of nanometers, and at lower magnifications, the length of CNTs could be up to several micrometers. The black nanoparticles encapsulated within the CNTs were related to reduced iron (**Fig. 6(a)** inset, the lattice fringe was 0.204 nm), and the nanoparticles were mainly concentrated in the top or the middle of the CNTs. It appears that the tip growth mechanism was the dominant growth mode rather than the base growth mechanism. It seems like that Fe based catalyst played a more important role compared with the type of plastics regarding the growth mechanism of carbon nanotubes. The lamellar material associated with the particles corresponded to graphite carbon layers (**Fig. 6(b)** and **6(c)** inset). Furthermore, for the carbon deposition on the catalysts produced from PP shown in **Fig. 6(a)**, there were more CNTs intertwined with each other. This might be attributed to the higher content of ash (**Table 1**), which may have partly poisoned the metal catalyst particles [36], which is unfavorable for the normal growth of carbon nanotubes, and thereby the CNTs were more closely entangled

with each other. But for the deposited carbon from HDPE and LDPE shown in **Fig. 6(b)** and **6(c)**, better dispersed and cleaner carbon nanotubes could be observed compared with that from PP. Similar results were obtained by Yang et al. [37]. In addition, as shown in **Fig. 6(d)** and **6(e)**, in addition to CNTs, amorphous carbon was observed from the carbon deposition from HIPS (**Fig. 6(d)**) and GPPS (**Fig. 6(e)**), which could be related to the intrinsic structure of PS. High pyrolysis temperature promotes the decomposition of PS into aromatic hydrocarbons [38], and part of the aromatic hydrocarbons act as precursors for the production of amorphous carbon in the presence of catalyst. Aboul-Enein et al. [24] also reported that PP was not a good raw material for the production of carbon nanotubes due to the low quality and purity of the CNTs produced.

In order to further distinguish the relative amounts of the different types of carbon deposits on the catalyst, temperature programmed oxidation of the deposits was undertaken using thermogravimetric analysis (TG). As shown in **Fig. 7(a)**, when the temperature was under 450 °C, the mass of all the samples changed very little. With the increase in temperature, there was a decrease in the mass, especially for the deposited carbons from HIPS and GPPS. However, the mass reduction in the carbon deposits produced from the polyolefin plastics (PP and PE) lagged slightly, which could be attributed to the large number of stable graphite carbon materials (mainly CNTs). Furthermore,, larger weight loss was obtained for the carbons related to HIPS and GPPS. These results are consistent with the products distribution shown in **Fig. 3**. It has been reported that the type of deposited carbon could be determined and calculated

according to oxidizing temperature [39]. Weight loss between 450~650 °C was related to amorphous type carbon, and weight loss higher than 650 °C corresponded to graphite. As shown in **Fig. 7(b)**, PP and PE produced a higher proportion of graphite type carbon (over 75%), in which the highest proportion of graphite carbon was obtained from HDPE (~77.8%). Simultaneously, around 20% amorphous carbon were also detected according to the TG results. The amorphous carbon might be originated from oligomerizations reaction of lower molecular weight polycyclic aromatic compounds[40]. But for HIPS and GPPS, almost half of the deposited carbon was amorphous carbon, at 48.0% and 47.4% for HIPS and GPPS, respectively. The existence of a large amount of amorphous carbon further confirmed the results of TEM shown in **Fig. 6**. This might be ascribed to the widespread aromatic hydrocarbons produced during the pyrolysis of PS, which was difficult to participate in the formation process of CNTs due to the stable structure compared with micromolecule hydrocarbons. The results also shown that PE or PP might be more appropriate raw materials for the production of CNTs compared with HIPS and GPPS.

XRD and Raman spectra of the reacted catalysts produced from the pyrolysis-catalysis of the different types of waste plastics are presented in **Fig.8**. As can be seen from **Fig.8(a)**, a large number and the type of peaks were essentially unchanged. All the peaks could be divided into three groups, corresponding to C, Fe and Al₂O₃, respectively. The peaks at about 2θ 26° and 43° are associated with the (002) lattice plane of graphite and (100) lattice plane of Fe, respectively. The related physical and chemical parameters were calculated from Scherrer-Formula and Brag's law

(shown in **Table 2**). The D_{Fe} for iron in the used catalysts produced from the pyrolysis-catalysis of the different plastics changed from 10.978 to 11.492 nm. It seems that the size of iron particles remained almost the same, which might suggest that changes in the reducing gases have little effect on the reduction of iron oxide and the corresponding particle size of iron. For the graphite peak, shown in **Table 2**, d_{002} changed from 0.340 to 0.344 nm, which revealed a certain deviation from the theoretical value of 0.335 nm [41]. This might be attributed to the structural defects in the carbon nanotubes. In addition, the degree of graphitization (g^d) and carbon layer number (N) of the deposited carbon were also calculated. The results showed that carbon deposition produced from the pyrolysis-catalysis of polyolefin plastics produced a higher degree of graphitization, especially for the carbon deposits in relation to processing of PP, showing the highest value of g^d of 0.364. But the relatively lower degree of graphitization obtained from PS deposited carbon, was consistent with other reports [24]. Teblum et al. found that aromatic hydrocarbon, the unbranched aromatic hydrocarbons in particular, have a negative effect on CNT growth due to its high chemical and thermal stability [42]. Similar results were also obtained by Li [43] and Brenner [44]. In addition, the lower degree of graphitization might also be attributed to the formation of more amorphous carbon from the oligomerization of benzene and its derivatives [40, 45]. Furthermore, Raman spectrometry characterization was also executed to evaluate the properties of the carbon deposits. Notably, the I_D/I_G (the intensity ratio of D to G bands) is used to estimate the number of disordered and defected sites in the carbon structure, and I_G/I_G (the intensity ratio

of G' and G bands) is used to describe the purity of the carbon nanotubes produced [46]. As shown in **Fig.8(b)**, the carbon deposits produced with PP revealed a lower ratio of I_D/I_G (0.52) and higher ratio of I_G/I_G (0.64), indicating a higher degree of graphitization of the produced carbon deposits produced from the pyrolysis-catalysis of PP. This was consistent with the results produced from XRD analysis of the used catalysts (**Table2**). The deposited carbon produced from HIPS and GPPS exhibited a relatively higher ratio of I_D/I_G and lower ratio of I_G/I_G than other samples, indicating the existence of amorphous carbon and the lower purity of CNTs produced. The TG results also confirmed that more amorphous carbon was obtained from PS.

3.3 Possible reaction mechanisms for the catalytic conversion process.

As discussed above, gaseous, liquid and solid products were obtained from pyrolysis-catalysis of waste plastics in the presence of Fe/Al₂O₃ catalyst. Based on the yield distribution and chemical compositions of the products, possible reaction pathways for the thermal conversion process of the different types of plastics are proposed in **Fig. 9**). PP and PE are mainly cracked into propylene and ethylene by random scission at high temperature [3]. The volatiles from PP and PE are transferred into the catalyst reactor and the catalytic reactions over Fe/Al₂O₃ occur. Propylene, ethylene and olefins are converted to CNTs via bond breaking and the carbon dissolving capacity of iron particles [47]. Compared with propylene, smaller molecules, such as the ethylene, cracked from HDPE or LDPE might be more actively involved in the catalytic deposition process, leading to a higher yield of solid carbon

deposition and eventually formation of CNTs. The other H atoms are mainly released in the form of H₂ [48]. Simultaneously, there are also some light olefins converted to monocyclic aromatic compounds by cyclization or Diels-Alder reaction and dehydrogenation [49]. Monocyclic aromatic compounds could further transform to polycyclic aromatic compounds through oligomerization reaction, and the produced aromatic hydrocarbons dominates in the liquid product. But for PS, aromatic hydrocarbons (mainly styrene) are the main products of polymer degradation by random scission and chain-end scission [18]. A small fraction of aromatics might go through the cracking of the branched chain, and the branched molecule could react in the pathway proposed before. But more aromatic hydrocarbons might transform to polycyclic aromatics through oligomerization reactions which are the important components of liquid products and even the precursors of coke [35], leading to more formation of amorphous carbon.

4 Conclusions

In conclusion, the production of products like carbon nanotubes via the pyrolysis-catalysis of different types of waste plastics (PP, HDPE, LDPE, HIPS and GPPS) have been investigated in the presence of an Fe/Al₂O₃ catalyst. The results showed that PP and PE produced higher yields of gaseous products (over 40 wt.%) and lower gaseous products were obtained from PS, but the H₂ content of the produced gases significantly improved, resulting in over 70 vol.% in the gaseous products from HIPS and GPPS. The liquid products from the different plastics

contained abundant aromatic hydrocarbons, with the highest produced with the PS plastics. As for solid carbon products, more carbon deposits on the catalyst was obtained from PS, especially HIPS (49.4 wt.%). However, less graphite type carbon was gathered from PS which was related to the difference of the intrinsic structure and further reflected the diverse carbon deposition mechanisms for PS (HIPS and PGGs) and polyolefin (PP, HDPE and LDPE) plastics.

Acknowledgements

The authors wish to express their sincere thanks for the financial support from the National Key Research and Development Program of China (2018YFC1901204), the National Natural Science Foundation of China (51806077 and 51861130362), China Postdoctoral Science Foundation (2018M640696), the Foundation of the State Key Laboratory of Coal Combustion (FSKLCCA1805). The experiment was also assisted by the Analytical and Testing Center in Huazhong University of Science & Technology (<http://atc.hust.edu.cn>, Wuhan 430074 China) and ZHONG KE BAI CE (<http://www.zkbaice.com/>).

Reference

- [1] Quesada, L., Calero, M., Martín-Lara, M. A., Pérez, A., Blázquez, G., *Energy*, 186 (2019), pp. 115874
- [2] Caroline, A. Philippa, B. , *Science*, 360 (2018), pp. 1310
- [3] Sharuddin, S., Abnisa,, Daud, F. W., Aroua, M. , *Energy Convers. Manage.*, 115 (2016), pp. 308-326
- [4] Geyer, R., Jambeck, J. R., Law, K. L. , *Sci. Adv.*, 3 (2017), pp. 1-5
- [5] Saleem, J., Adil Riaz, M., Gordon, M., *J Hazard Mater*, 341 (2018), pp. 424-437
- [6] Baroulaki, I., Karakasi, O., Pappa, G., Tarantili, P. A., Economides, D., Magoulas, K., *Composites Part A: Applied Science and Manufacturing*, 37 (2006), pp. 1613-1625
- [7] Jambeck, J. R., Geyer, R., Wilcox, C., Siegler, T R., Perryman, M., Andrady, A., Narayan, R., Law. K., *SCIENCE*, 347 (2015), pp. 768-771
- [8] Yao, D., Wu, C., Yang, H., Zhang, Y., Nahil , M. A., Chen, Y., Williams, P. T., Chen, H. , *Energy Convers. Manage.*, 148 (2017), pp. 692-700
- [9] Barbarias, I. . Lopez, G., Artetxe, M., Arregi, A., Bilbao, J., Olazar, M., *Energy Conversion and Management*, 156 (2018), pp. 575-584
- [10] Wu, C., Williams, P. , *Appl. Catal. B: Environ.*, 90 (2009), pp. 147-156

-
- [11] Miskolczi, N., Angyal, A., Bartha, L., Valkai, I., *Fuel Processing Technology*, 90 (2009), pp. 1032-1040
- [12] Zhang, Y., Duan, D., Lei, H., Villota, E., Ruan, R., *Applied Energy*, 251 (2019), pp. 113337
- [13] Quesada, L. Pérez, A. Godoy, V. Peula, F. J. Calero, M. Blázquez, G., *Energy Conversion and Management*, 188 (2019), pp. 19-26
- [14] Nahil, M., Wu, C., Williams, P., *Fuel Processing Technology*, 130 (2015), pp. 46-53
- [15] Veksha, A., Yin, K., Moo, J., Oh, W., Ahamed, A., Chen, W., Weerachanchai, P., Giannis, A., Lisak, G., *J. Hazard. Mater.*, (2019), pp. 121256
- [16] Jia, J., Veksha, A., Lim, T., Lisak, G., *Journal of Cleaner Production*, 258 (2020), pp. 120633
- [17] Wu, C., Williams, P. T., *Applied Catalysis B: Environmental*, 87 (2009), pp. 152-161
- [18] Park, Ki., Jeong, Y., Guzelciftci, B., Kim, J., *Applied Energy*, 259 (2020), pp. 114240
- [19] Huo, E., Lei, H., Liu, C., Zhang, Y., Xin, L., Zhao, Y., Qian, M., Zhang, Q., Lin, X., Wang, C., Mateo, W., Villota, E. M., Ruan, R., *Sci Total Environ*, 727 (2020), pp. 138411
- [20] Zhang, J., Zhang, L., Yang, H., Kong, Q., Liu, Y., Yuan, A., *CrystEngComm*,

16 (2014), pp. 8832-8840

[21] Yao, D., Zhang, Y., Williams, P. T., Yang, H., Chen, H., *Applied Catalysis B: Environmental*, 221 (2018), pp. 584-597

[22] Saad, J., Williams, P.T., *Energy & Fuels*, 30 (2016), pp. 3198-3204

[23] Miandad, R. Barakat, M. A. Rehan, M. Aburiazaiza, A. S. Ismail, I. M. I. Nizami, A. S., *Waste Manag*, 69 (2017), pp. 66-78

[24] Aboul-Enein, Ateyya A., Awadallah, Ahmed E., Abdel-Rahman, Adel A. H., Haggag, Ahmed M., *Fullerenes, Nanotubes and Carbon Nanostructures*, 26 (2018), pp. 443-450

[25] Cai, N., Xia, S., Zhang, X., Meng, Z., Bartocci, P., Fantozzi, F., Chen, Y., Chen, H., Williams, P. T., Yang, H., *ChemSusChem*, 13 (2020), pp. 938-944

[26] Wu, J., Xia, M., Zhang, Xi., Chen, Y., Sun, F., Wang, X., Yang, H., Chen, H., *Journal of Power Sources*, 455 (2020), pp. 227982

[27] Cui, H., Wu, X., Chen, Y., Boughton, R. I., *Materials Research Bulletin*, 50 (2014), pp. 307-311

[28] Yao, D., Yang, H., Chen, H., Williams, T., *Appl. Catal. B: Environ.*, 239 (2018), pp. 565-577

[29] Hernadi K., Fonseca A, Nagy B., Siska A, Kiricsi I., *Applied Catalysis A: General*, 199 (2000), pp. 245-255

[30] Miandad, R., Barakat, M. A., Aburiazaiza, Asad S., Rehan, M., Ismail, I. M.

I., Nizami, A. S., *International Biodeterioration & Biodegradation*, 119 (2017), pp. 239-252

[31] Wu, C., Williams, P.T., *Fuel*, 89 (2010), pp. 3022-3032

[32] Pinto, F. Costa, P. Gulyurtlu, I. Cabrita, I., *JAAP*, 51 (1999), pp. 39-55

[33] Alayoglu, S., Nilekar, A. U., Mavrikakis, M., Eichhorn, B., *Nature materials*, 7 (2008), pp. 333-338

[34] Gao, Y., Wang, X., Chen, Y., Li, P., Liu, H., Chen, H., *Energy*, 122 (2017), pp. 482-491

[35] Chi, Y., Xue, J., Zhuo, J., Zhang, D., Liu, M., Yao, Q., *Sci Total Environ*, 633 (2018), pp. 1105-1113

[36] Yildiz, G., Ronsse, F., Venderbosch, R., Duren, R., Kersten, S. R. A., Prins, W., *Applied Catalysis B: Environmental*, 168-169 (2015), pp. 203-211

[37] Yang, Z., Zhang, Q., Luo, G., Huang, J., Zhao, M., Wei, F., *Applied Physics A*, 100 (2010), pp. 533-540

[38] Wang, J., Jiang, J., Sun, Y., Zhong, Z., Wang, X., Xia, H., Liu, G., Pang, S., Wang, K., Li, M., Xu, J., Ruan, R., Ragauskas, A., *Energy Conversion and Management*, 200 (2019), pp. 112088

[39] Yang, R., Chuang, K., Wey, M., *Energy & Fuels*, 29 (2015), pp. 8178-8187

[40] Chen, X., Che, Q., Li, S., Liu, Z., Yang, H., Chen, Y., Wang, X., Shao, J., Chen, H., *Fuel Processing Technology*, 196 (2019), pp. 106180

-
- [41] Marjolein L. Toebes, Jos A. van Dillen, Krijn P. de Jong, *Journal of Molecular Catalysis A: Chemical*, 173 (2001), pp. 75-98
- [42] Teblum, E., Itzhak, A., Shawat-Avraham, E., Muallem, M., Yemini, R., Nessim, G., *Carbon*, 109 (2016), pp. 727-736
- [43] Li, H., He, D., Li, T., Genestoux, M., Bai, J., *Carbon*, 48 (2010), pp. 4330-4342
- [44] Brenner, M., Boddu, V., Kumar, A., *Applied Physics A*, 117 (2014), pp. 1849-1857
- [45] Deng, Q., Zhang, X., Wang, L., Zou, J., *Chemical Engineering Science*, 135 (2015), pp. 540-546
- [46] Cai, N., Yang, H., Zhang, X., Xia, S., Yao, D., Bartocci, P., Fantozzi, F., Chen, Y., Chen, H., Williams, P. T., *Waste Manag*, 109 (2020), pp. 119-126
- [47] Zhou, L., Enakonda, L., Harb, M., Saih, Y., Aguilar-Tapia, A., Ould-Chikh, S., Hazemann, J., Li, J., Wei, N., Gary, D., Del-Gallo, P., Basset, J., *Applied Catalysis B: Environmental*, 208 (2017), pp. 44-59
- [48] Wunderlich, W., *Diamond and Related Materials*, 16 (2007), pp. 369-378
- [49] Park, K., Jeong, Y., Guzelciftci, B., Kim, J., *Energy*, 166 (2019), pp. 343-351

Table 1. Proximate and ultimate analysis of the waste plastics.

Sample	Ultimate analysis(wt.%) _{db}				Proximate analysis(wt.%) _{ar}			
	C	H	S	O*	Moisture	Ash	Volatiles	Fixed Carbon
PP	85.18	13.74	0.17	0.87	0.04	0.06	99.87	0.03
HDPE	85.02	14.60	0.21	0.16	0.00	0.01	99.81	0.18
LDPE	85.11	14.49	0.19	0.19	0.03	0.04	99.71	0.22
HIPS	91.36	7.51	0.69	0.51	0.17	0.02	99.65	0.06
GPPS	91.31	7.70	0.63	0.40	0.15	0.03	99.60	0.12

* Calculated by difference

Table 2. Data on graphitization and Fe particles from XRD analysis of the reacted catalysts.

Sample	D _C (nm)	d ₀₀₂ (nm)	g ^d	N	D _{Fe} (nm)
R-PP	7.759	0.344	0.364	22.574	10.978
R-HDPE	8.570	0.341	0.331	25.120	11.346
R-LDPE	9.270	0.341	0.355	27.184	11.358
R-HIPS	7.735	0.342	0.259	22.601	11.354
R-GPPS	8.749	0.342	0.205	25.600	11.492

FIGURE CAPTIONS

Fig.1. Schematic diagram of the pyrolysis-catalysis reactor system

Fig. 2(a) N₂absorption and desorption curve 2(b) Pore size distribution 2(c) SEM image 2(d) XRD spectrum of fresh Fe/Al₂O₃catalyst, respectively.

Fig. 3. Products distribution of pyrolysis-catalysis products in relation to different types of waste plastics.

Fig. 4. Composition of gaseous products from the pyrolysis-catalysis of different types of waste plastics.

Fig. 5. Carbon number (% area) and the corresponding components of the liquid products from the pyrolysis-catalysis of different types of plastics.

Fig. 6. TEM images of the carbon deposits from the reacted catalysts from the pyrolysis-catalysis of the different type of waste plastics (Fig. 6(a), PP; Fig. 6(b) HDPE; Fig 6(c), LDPE; Fig 6(d) HIPS; Fig 6(e), GPPS)

Fig. 7(a) TGA thermograms and 7(b) proportion of different carbon types from the deposited carbon residue on the reacted catalysts ('R-PLASTIC' relates to the carbon residue deposited on the catalysts related to each plastic type).

Fig. 8(a) X-ray diffraction and 8(b) Raman spectrum of the reacted catalysts.

Fig. 9. Possible reaction pathways for the catalytic thermal conversion process of different types of plastics.

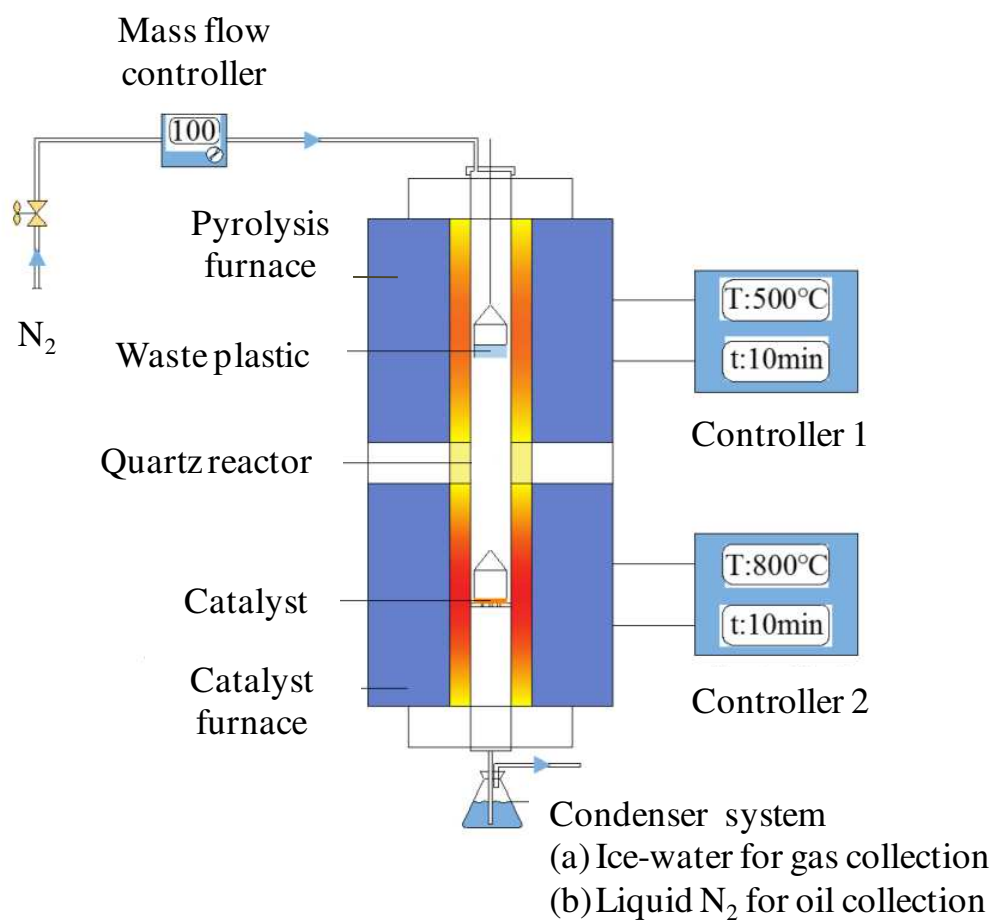


Fig.1. Schematic diagram of the pyrolysis-catalysis reactor system

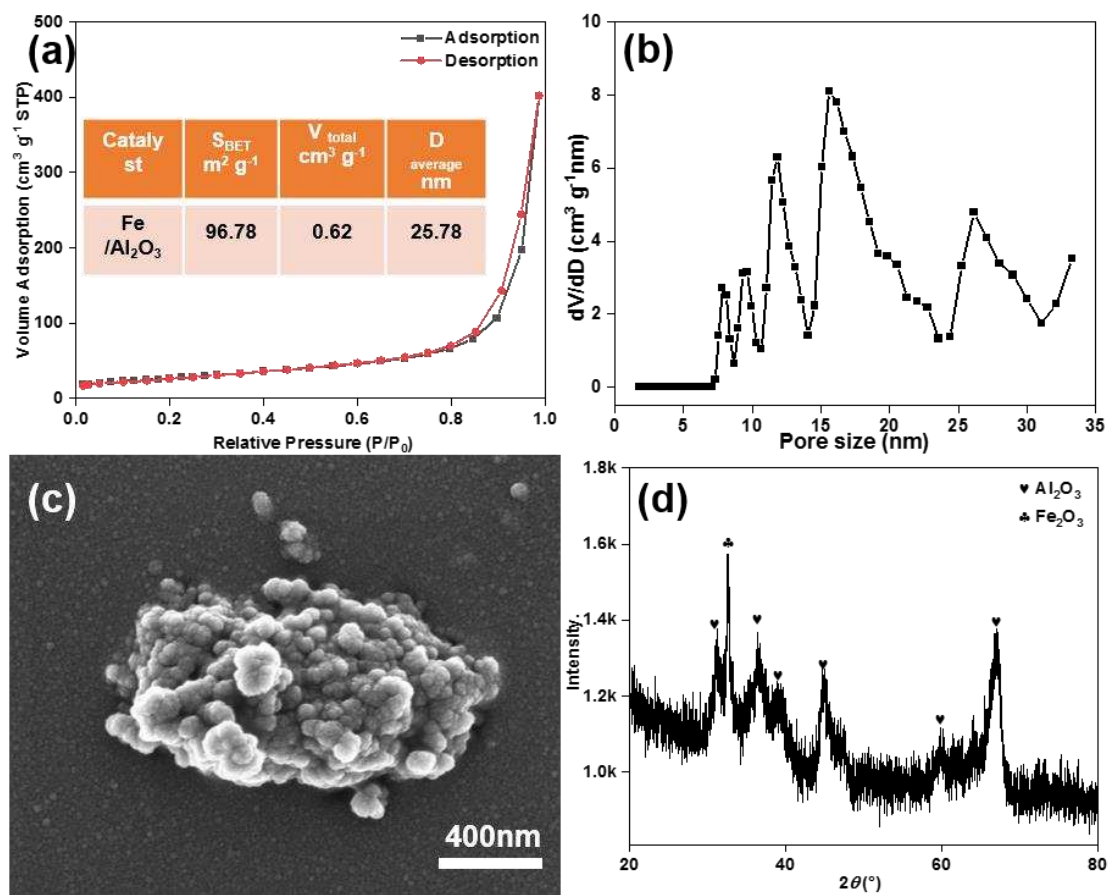


Fig. 2(a) N₂ adsorption and desorption curve 2(b) Pore size distribution 2(c) SEM image 2(d) XRD spectrum of fresh Fe/Al₂O₃ catalyst, respectively.

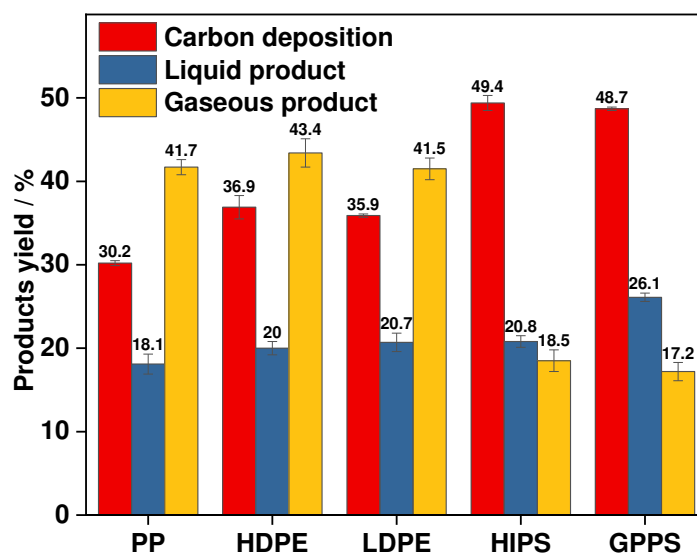


Fig. 3. Products distribution of pyrolysis-catalysis products in relation to different types of waste plastics.

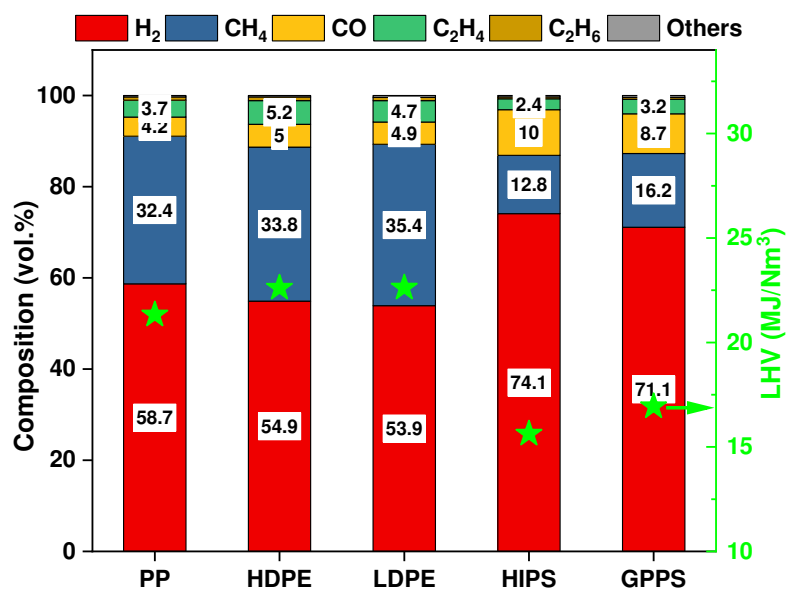


Fig. 4. Composition of gaseous products from the pyrolysis-catalysis of different types of waste plastics.

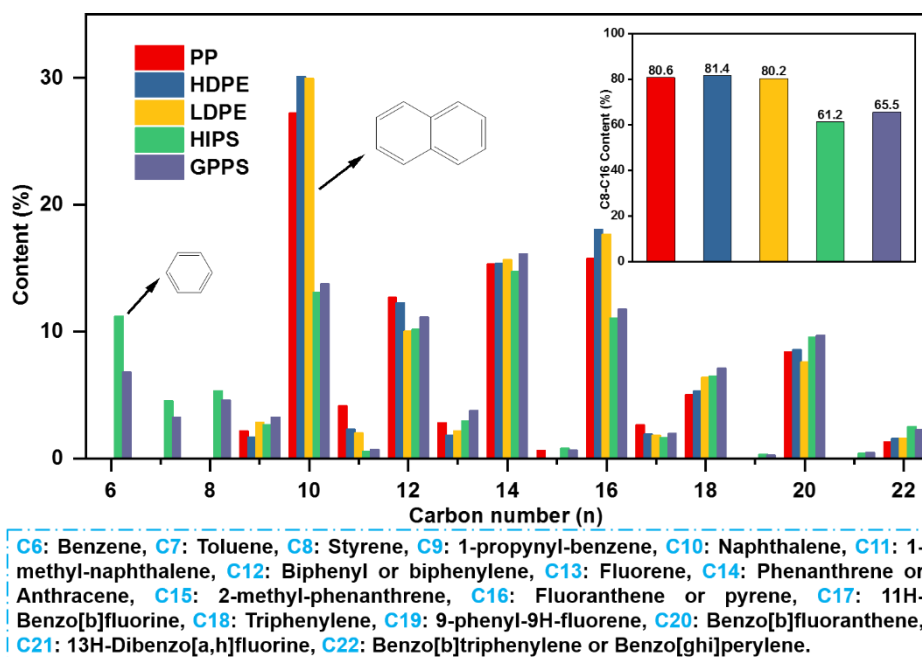


Fig. 5. Carbon number (% area) and the corresponding components of the liquid products from the pyrolysis-catalysis of different types of plastics.

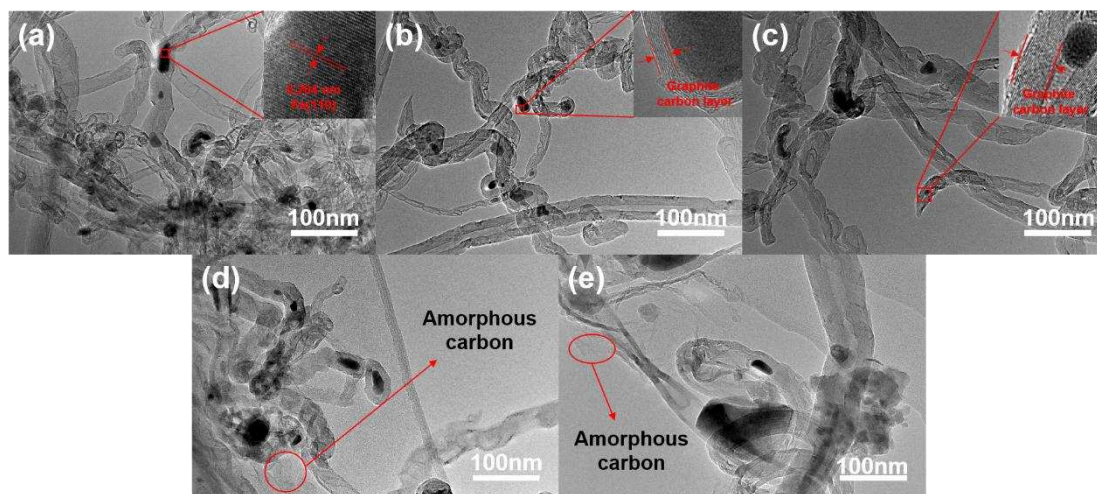


Fig. 6. TEM images of the carbon deposits from the reacted catalysts from the pyrolysis-catalysis of the different type of waste plastics (Fig. 6(a), PP; Fig. 6(b) HDPE; Fig 6(c), LDPE; Fig 6(d) HIPS; Fig 6(e), GPPS)

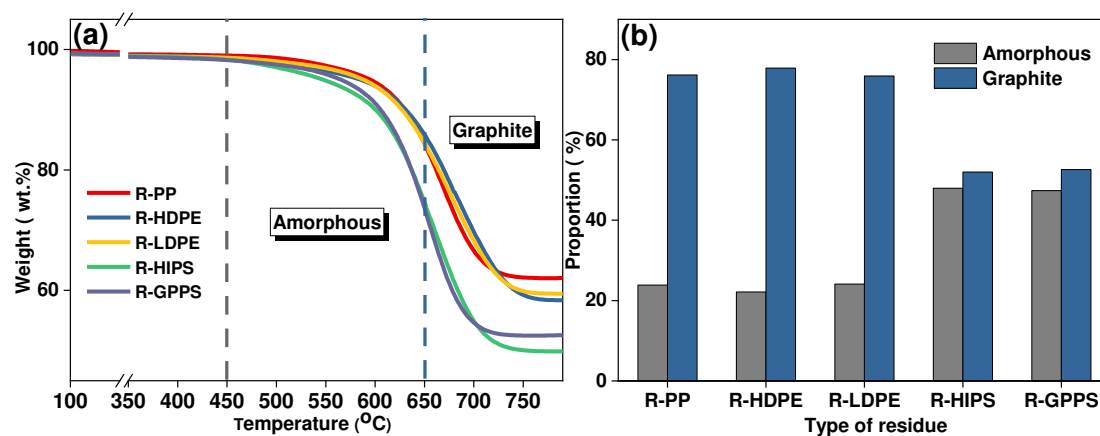


Fig. 7. (a) TGA thermograms and (b) proportion of different carbon types from the deposited carbon residue on the reacted catalysts ('R-PLASTIC' relates to the carbon residue deposited on the catalysts related to each plastic type).

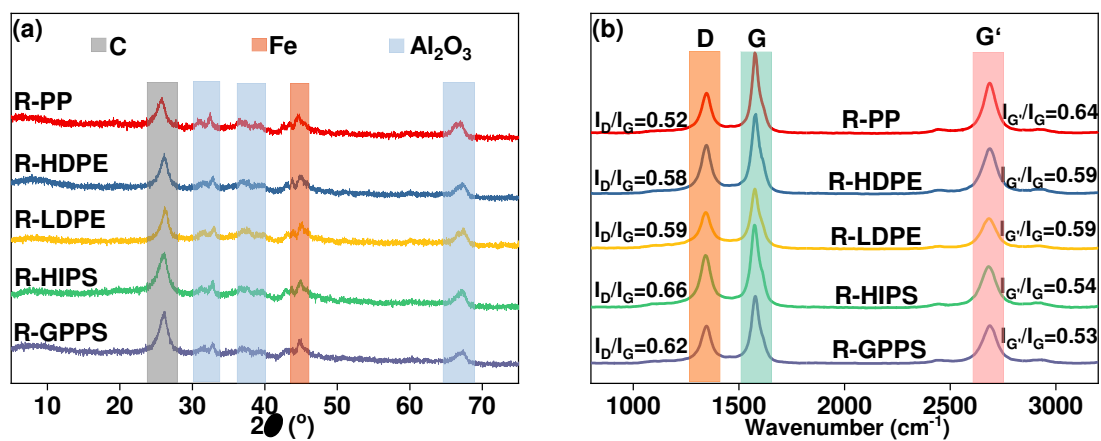


Fig.8. (a) X-ray diffraction and (b) Raman spectrum of the reacted catalysts.

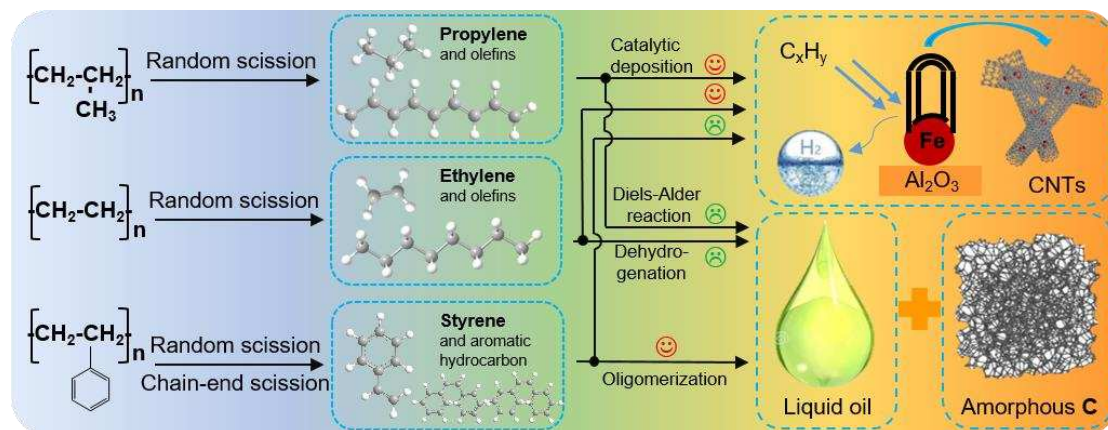


Fig.9. Possible reaction pathways for the catalytic thermal conversion process of different types of plastics.